Article

Uracil-Directed Ligand Tethering: An Efficient Strategy for Uracil DNA Glycosylase (UNG) Inhibitor Development

Yu Lin Jiang, Daniel J. Krosky, Lauren Seiple, and James T. Stivers

J. Am. Chem. Soc., **2005**, 127 (49), 17412-17420• DOI: 10.1021/ja055846n • Publication Date (Web): 15 November 2005

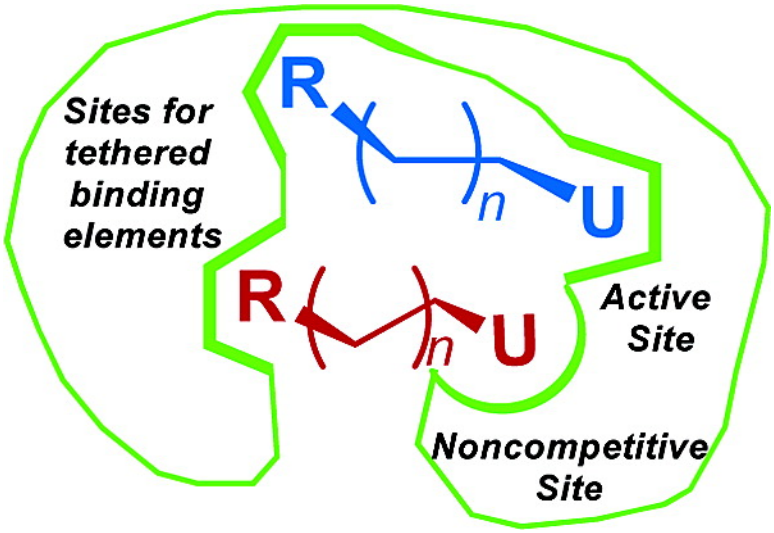

More About This Article

Additional resources and features associated with this article are available within the HTML version:

- Supporting Information
- Links to the 2 articles that cite this article, as of the time of this article download
- Access to high resolution figures
- Links to articles and content related to this article
- Copyright permission to reproduce figures and/or text from this article

View the Full Text HTML

J|A|C|S
ARTICLES
Published on Web 11/15/2005

Uracil-Directed Ligand Tethering: An Efficient Strategy for Uracil DNA Glycosylase (UNG) Inhibitor Development

Yu Lin Jiang, Daniel J. Krosky, Lauren Seiple, and James T. Stivers*

Contribution from the Department of Pharmacology and Molecular Sciences, Johns Hopkins University School of Medicine, 725 North Wolfe Street, Baltimore, Maryland 21205

Received August 25, 2005; E-mail: jstivers@jhmi.edu

Abstract: Uracil DNA glycosylase (UNG) is an important DNA repair enzyme that recognizes and excises uracil bases in DNA using an extrahelical recognition mechanism. It is emerging as a desirable target for small-molecule inhibitors given its key role in a wide range of biological processes including the generation of antibody diversity, DNA replication in a number of viruses, and the formation of DNA strand breaks during anticancer drug therapy. To accelerate the discovery of inhibitors of UNG we have developed a uracil-directed ligand tethering strategy. In this efficient approach, a uracil aldehyde ligand is tethered via alkyloxyamine linker chemistry to a diverse array of aldehyde binding elements. Thus, the mechanism of extrahelical recognition of the uracil ligand is exploited to target the UNG active site, and alkyloxyamine linker tethering is used to randomly explore peripheral binding pockets. Since no compound purification is required, this approach rapidly identified the first small-molecule inhibitors of human UNG with micromolar to submicromolar binding affinities. In a surprising result, these uracil-based ligands are found not only to bind to the active site but also to bind to a second uncompetitive site. The weaker uncompetitive site suggests the existence of a transient binding site for uracil during the multistep extrahelical recognition mechanism. This very general inhibitor design strategy can be easily adapted to target other enzymes that recognize nucleobases, including other DNA repair enzymes that recognize other types of extrahelical DNA bases.

Introduction

DNA repair pathways have been traditionally viewed as the cellular quality control machinery that preserves the coding potential of genomes.[1] However, there is emerging recognition that the repair mechanisms evolved to prevent accumulation of the RNA base uracil in DNA play a much broader role in a number of important areas of biomedicine that are divergent from genome preservation. Remarkable examples include the role of the uracil excision repair machinery in the process of generating genetic diversity during antibody maturation in B cells,[2−4] the importance of uracil incorporation and removal in the life cycles of herpes,[5] cytomegalo,[6] pox,[7,8] and type 1 human immunodeficiency viruses (HIV-1),[9] and the essential role of this pathway in generating pharmacologically active single and double strand DNA breaks during chemotherapy treatment with 5-flurouracil and methotrexate.[10,11] The key enzyme player in all of these remarkably diverse processes is uracil DNA glycosylase (UNG), which cleaves the glycosidic bond between the uracil base and the deoxyribose sugar in DNA by flipping the uracil nucleotide from the DNA duplex into the enzyme active site (Figure 1A).[12] Given that UNG is emerging as a very interesting pharmacologic target, we have sought out methods for the rapid and efficient identification of small-molecule ligands that could inhibit its activity. Although potent nucleic acid-based and proteinaceous inhibitors are available that target UNG,[13−17] there are no small-molecule inhibitors for this enzyme, and strategies for the discovery of such ligands are lacking.

One of the most exciting potential applications of small-molecule human UNG inhibitors are as antiretroviral agents. Recent findings have established that HIV-1 specifically packages human UNG (hUNG) into virus particles via interaction with the virus encoded integrase protein (Int) or perhaps a ternary complex between UNG, Int, and the viral Vpr

(1) Lindahl, T.; Wood, R. D. *Science* **1999**, *286*, 1897−1905.
(2) Di Noia, J.; Neuberger, M. S. *Nature* **2002**, *419*, 43−48.
(3) Imai, K.; Slupphaug, G.; Lee, W. I.; Revy, P.; Nonoyama, S.; Catalan, N.; Yel, L.; Forveille, M.; Kavli, B.; Krokan, H. E.; Ochs, H. D.; Fischer, A.; Durandy, A. *Nat. Immunol* **2003**, *4*, 1023−1028.
(4) Storb, U.; Stavnezer, J. *Curr. Biol.* **2002**, *12*, R725−727.
(5) Chen, R.; Wang, H.; Mansky, L. M. *J. Gen. Virol.* **2002**, *83*, 2339−2345.
(6) Prichard, M. N.; Duke, G. M.; Mocarski, E. S. *J. Virol.* **1996**, *70*, 3018−3025.
(7) De Silva, F. S.; Moss, B. *J. Virol.* **2003**, *77*, 159−166.
(8) Stuart, D. T.; Upton, C.; Higman, M. A.; Niles, E. G.; McFadden, G. *J. Virol.* **1993**, *67*, 2503−2512.
(9) Priet, S.; Gros, N.; Navarro, J. M.; Boretto, J.; Canard, B.; Querat, G.; Sire, J. *Mol. Cell* **2005**, *17*, 479−490.
(10) Ladner, R. D. *Curr. Protein Pept. Sci.* **2001**, *2*, 361−370.
(11) Tinkelenberg, B. A.; Hansbury, M. J.; Ladner, R. D. *Cancer Res.* **2002**, *62*, 4909−4915.
(12) Stivers, J. T.; Drohat, A. C. *Arch. Biochem. Biophys.* **2001**, *396*, 1−9.
(13) Bianchet, M. A.; Seiple, L. A.; Jiang, Y. L.; Ichikawa, Y.; Amzel, L. M.; Stivers, J. T. *Biochemistry* **2003**, *42*, 12455−12460.
(14) Jiang, Y. L.; Cao, C.; Stivers, J. T.; Song, F.; Ichikawa, Y. *Bioorg. Chem.* **2004**, *32*, 244−262.
(15) Krosky, D. J.; Song, F.; Stivers, J. T. *Biochemistry* **2005**, *44*, 5949−5959.
(16) Sekino, Y.; Bruner, S. D.; Verdine, G. L. *J. Biol. Chem.* **2000**, *275*, 36506−36508.
(17) Putnam, C. D.; Shroyer, M. J. N.; Lundquist, A. J.; Mol, C. D.; Arvai, A. S.; Mosbaugh, D. W.; Tainer, J. A. *J. Mol. Biol.* **1999**, *287*, 331−346.

10.1021/ja055846n CCC: $30.25

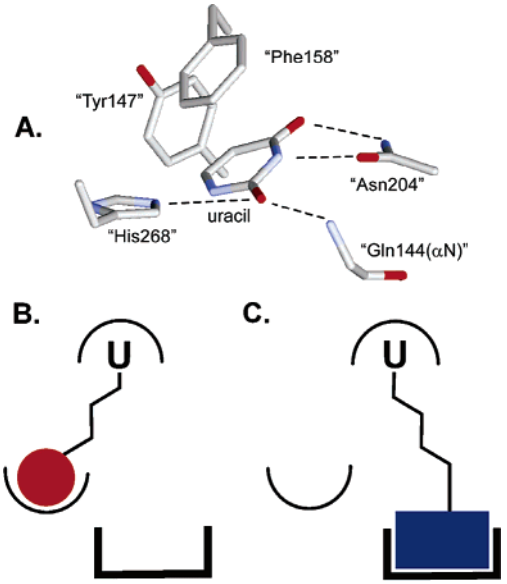

Figure 1. Extrahelical binding of uracil to the UNG active site and the general strategy for uracil-directed ligand tethering. (A) Structure of UNG bound to uracil is shown (pdb code 2eug). The residue numbering is for the human enzyme. (B, C) The uracil ligand (U) that targets the UDG active site is covalently tethered to two different ligands that can interact with distinct binding surfaces near the active site.

protein.[5,18−25] hUNG is required for infection of nondividing cells such as macrophages and resting T cells and helps maintain a viral reservoir in the host that is crucial for virus spread to the lymphoid organs and T-helper lymphocytes and, ultimately, AIDS pathogenesis.[20,26] UNG is apparently recruited to minimize uracil incorporation into the viral genome in these cells, which have naturally high levels of dUTP, a good substrate for the viral reverse transcriptase.[27] In the absence of UNG, the HIV-1 mutation rate is found to increase by 18-fold resulting in extremely inefficient virus replication in nondividing cells,[20] and the virus particles produced from UNG-depleted cells are incapable of infecting new target cells.[9,28] Pharmacologic targeting of a human enzyme required for virus infectivity is extremely attractive because such a target would not be susceptible to the same high mutagenesis rate and resulting drug resistance as viral encoded proteins.[29] Targeting the human enzyme is a viable therapeutic strategy because it is not an essential enzyme. Thus, UNG knock-out mice display no remarkable phenotype, nor do UNG null yeast or human cell lines.[30]

Herein, we report an integrated high-throughput (HTP) platform for discovering small-molecule ligands that inhibit UNG. The strategy takes advantage of the extrahelical uracil recognition mechanism of UNG by using the specificity and binding energy of a uracil ligand to target the UNG active site[14,31,32] and then covalent tethering of random functional groups for exploration of nearby binding pockets (Figure 1B). Library members can be rapidly screened using a robust HTP activity assay, and initial hits are quickly optimized using subsequent structure−activity studies. This tethering approach, which uses efficient oxime chemistry (Figure 2), is related to the "combinatorial target-guided ligand assembly" method of Ellman et al.[33] but differs in that the uracil ligand specifically targets the active site rather than irrelevant regions of the enzyme. Thus, the hit-rate and binding affinities of early hits are higher than the more random approach of Ellman and colleagues. This synthetic and screening strategy should be easily adaptable for the discovery of inhibitors of other enzymes that recognize extrahelical bases in DNA or free nucleosides.

Results and Discussion

Synthesis of Uracil-Tethered Oxime Libraries and General Strategy. We sought an inhibitor development strategy that allowed rapid and economical synthesis of small-molecule ligands that explore binding sites near the UNG active site and which could be used directly in HTP screening applications without purification. One efficient synthesis strategy that meets these criteria is outlined in Figure 2. First, flexible diaminoalkanediol linkers of variable length are synthesized from the corresponding dibromoalkanes (Figure 2A). Then the linkers are used to tether uracil aldehyde binding elements (**1**−**3**) to a library of aldehyde binding elements (RCHO) via the formation of stable oxime linkages (Figure 2B). Each tethering reaction is carried out in one well of a 96-well microtiter plate that contains one equivalent uracil aldehyde, one equivalent RCHO library member, and a mixture of diaminoalkanediol linkers (n = 2−6). The reactions typically proceed to 85−99% completion after overnight incubation (DMSO solvent, 37 °C) and produce a 1:2:1 statistical mixture of the homodimeric (U∧U, R∧R) and heterodimeric (U∧R) oximes for each of the five linker lengths present (see Experimental Section and Supporting Imformation Figure S1). Although two geometric configurations are possible, oxime derivatives with bulky substituents are generally found to be ≥95% in the trans configuration.[34] The unpurified oxime mixtures were directly screened for inhibition of UNG at ∼100 μM total oxime concentration to ensure that each component in the mixture is present at a concentration in the range 5−10 μM. If significant inhibition is observed by any mixture, the linker length and RCHO binding element that gave rise to the inhibition can be identified by resynthesis of the individual oximes using a single linker length in each reaction (see below).

An important aspect of this approach is that the uracil homodimers present in some reaction mixtures are inhibitory even in the absence of any active heterodimer. For instance,

(18) Bouhamdan, M.; Benichou, S.; Rey, F.; Navarro, J. M.; Agostini, I.; Spire, B.; Camonis, J.; Slupphaug, G.; Vigne, R.; Benarous, R.; Sire, J. *J. Virol.* **1996**, *70*, 697−704.
(19) BouHamdan, M.; Xue, Y.; Baudat, Y.; Hu, B.; Sire, J.; Pomerantz, R. J.; Duan, L. X. *J. Biol. Chem.* **1998**, *273*, 8009−8016.
(20) Chen, R.; Le Rouzic, E.; Kearney, J. A.; Mansky, L. M.; Benichou, S. *J. Biol. Chem.* **2004**, *279*, 28419−28425.
(21) Klarmann, G. J.; Chen, X.; North, T. W.; Preston, B. D. *J. Biol. Chem.* **2003**, *278*, 7902−7909.
(22) Mansky, L. M.; Preveral, S.; Selig, L.; Benarous, R.; Benichou, S. *J. Virol.* **2000**, *74*, 7039−7047.
(23) Payne, S. L.; Elder, J. H. *Curr. Protein Pept. Sci.* **2001**, *2*, 381−388.
(24) Selig, L.; Benichou, S.; Rogel, M. E.; Wu, L. I.; Vodicka, M. A.; Sire, J.; Benarous, R.; Emerman, M. *J. Virol.* **1997**, *71*, 4842−4846.
(25) Willetts, K. E.; Rey, F.; Agostini, I.; Navarro, J. M.; Baudat, Y.; Vigne, R.; Sire, J. *J. Virol.* **1999**, *73*, 1682−1688.
(26) Mansky, L. M.; Le Rouzic, E.; Benichou, S.; Gajary, L. C. *J. Virol.* **2003**, *77*, 2071−2080.
(27) Miller, R. J.; Cairns, J. S.; Bridges, S.; Sarver, N. *J. Virol.* **2000**, *74*, 7187−7195.
(28) Elder, R. T.; Zhu, X.; Priet, S.; Chen, M.; Yu, M.; Navarro, J. M.; Sire, J.; Zhao, Y. *Biochem. Biophys. Res. Commun.* **2003**, *306*, 693−700.
(29) Lau, A.; Swinbank, K. M.; Ahmed, P. S.; Taylor, D. L.; Jackson, S. P.; Smith, G. C.; O'Connor, M. J. *Nat. Cell Biol.* **2005**, *7*, 493−500.
(30) Nilsen, H.; Rosewell, I.; Robins, P.; Skjelbred, C. F.; Andersen, S.; Slupphaug, G.; Daly, G.; Krokan, H. E.; Lindahl, T.; Barnes, D. E. *Mol. Cell* **2000**, *5*, 1059−1065.
(31) Drohat, A. C.; Stivers, J. T. *Biochemistry* **2000**, *39*, 11865−11875.
(32) Drohat, A. C.; Stivers, J. T. *J. Am. Chem. Soc.* **2000**, 1840−1841.
(33) Maly, D. J.; Choong, I. C.; Ellman, J. A. *Proc. Natl. Acad. Sci. U.S.A.* **2000**, *97*, 2419−2424.
(34) Winans, K. A.; Bertozzi, C. R. *Chem. Biol.* **2002**, *9*, 113−129.

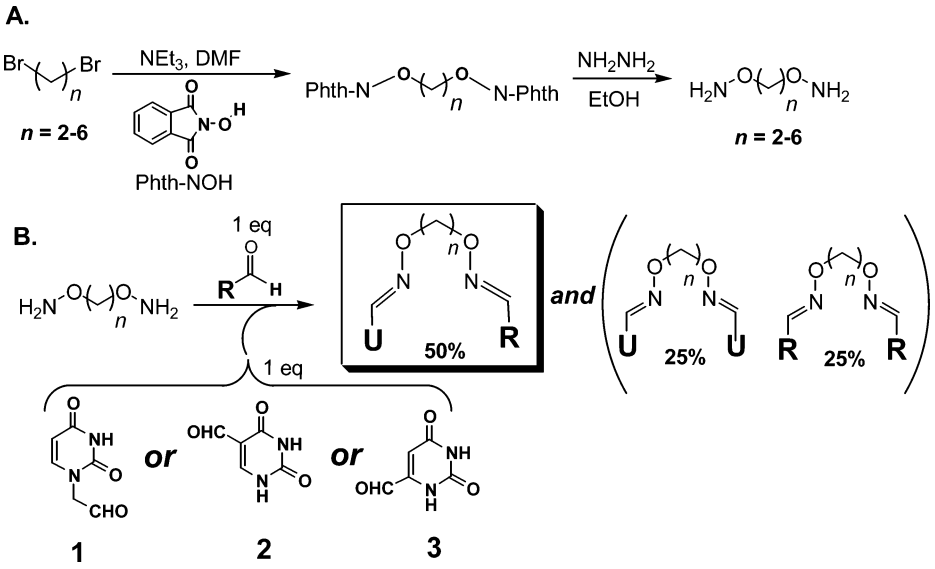

Figure 2. Synthesis of oxime libraries based on uracil and RCHO: (A) synthesis of diaminoalkanediol tethers of variable length; (B) construction of the uracil−oxime library based on the uracil aldehydes (**1**−**3**) and a series of aldehyde compounds (RCHO). The products consist of a 1:2:1 mixture of the heterodimer (U∧R) and the two homodimers (U∧U and R∧R) connected via alkane linkers of lengths 2−6. A 1 equiv amount of total diaminoalkanediol is added to each reaction. Each linker length is present at one-fifth of the total concentration.

the purified homodimers of various lengths that are based on 6-formyluracil (**3**) give rise to about 22% inhibition in all the mixtures based on **3** under the screening conditions (not shown). In contrast, the homodimers of **1** and **2** show no detectable inhibition under the same conditions. Thus, the screening assay must be robust enough to detect any *additional* inhibition resulting from an active heterodimer in the mixture. Spectroscopic results for determining the purity and composition of representative reaction mixtures are available (see Supporting Information).

High-Throughput Screening of Uracil−Oxime Libraries. To test this directed library approach, we tethered the three uracil aldehydes (**1**−**3**) shown in Figure 2 to 14 aldehyde binding elements (RCHO) using the variable-length diaminoalkanediol linkers (see Supporting Information Table S1 for RCHO structures). This library of uracil-linked binding elements was screened for inhibition of hUNG using a high-throughput molecular beacon activity assay **(**Figure 3**)**.[35] In this assay, one DNA strand is labeled with a fluorescent 5′-FAM and the complementary strand is modified with a 3′-dabsyl moiety that serves to efficiently quench the fluorescence of the FAM group through contact quenching. To increase stability, the two DNA strands are linked in a hairpin configuration using an 18 atom poly(ethylene glycol) linker. When the substrate DNA is exposed to UDG, multiple uracils are removed, and eventually the two paired strands of the hairpin spontaneously separate, thus removing the dabsyl quencher from the proximity of the FAM group and resulting in a 6-fold increase in the fluorescence of the system (Figure 3A). Under the assay conditions, the hairpin DNA substrate has a $K_m = 164 \pm 10$ nM and $k_{cat} = 0.33 \pm 0.01$ s^{-1} (Figure 3B). To enhance detection of competitive inhibitors during HTP screening we employed a molecular beacon substrate concentration equivalent to $1/3K_m$ (50 nM). Representative HTP screening results for several inactive and active oxime mixtures are shown in Figure 4 ([total oxime] = 100 μM).

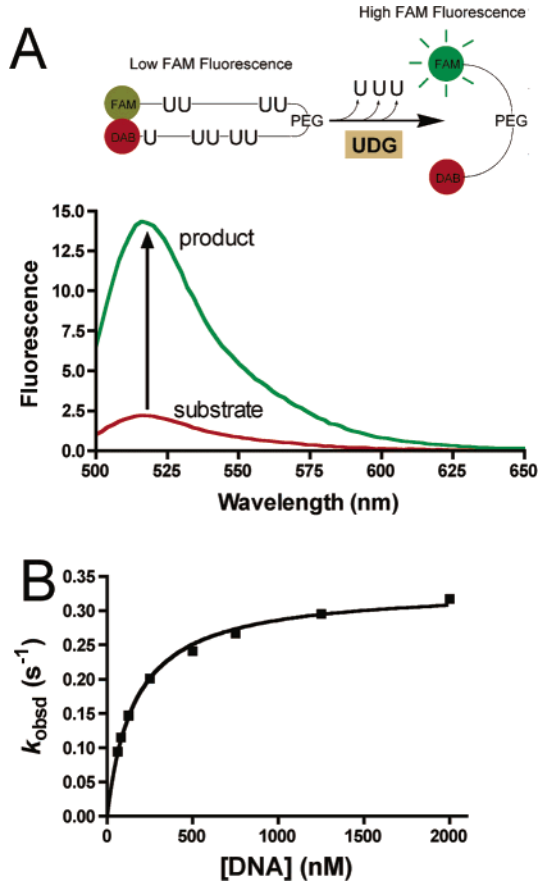

Figure 3. High-throughput (HTP) UDG kinetic assay. (A) The HTP assay relies on molecular beacon technology. Excision of multiple uracil bases by the enzyme destabilizes the hairpin structure thereby releasing the 5′-FAM fluorophore from the quenching effects of the 3′-dabsyl group. (B) Steady-state kinetic analysis is shown of the hUDG reaction using the molecular beacon hairpin substrate.

Several activity trends emerged immediately from the screening results shown in Figure 4. First, none of the mixtures derived from the uracil N1-acetaldehyde binding element (**1**) were inhibitory at the concentration used in the screen. In addition,

(35) Kwon, K.; Nagarajan, R.; Stivers, J. T. *Biochemistry* **2004**, *43*, 14994−15004.

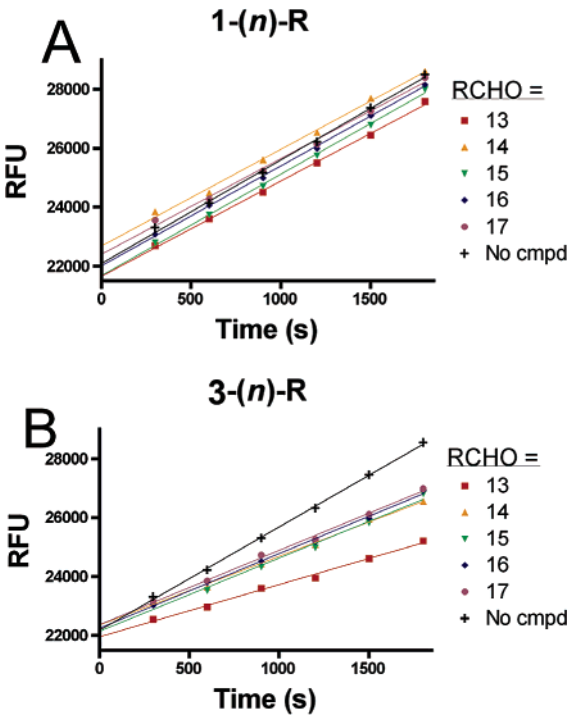

Figure 4. Representative HTP screening results using the molecular beacon substrate. (A) Screen of oxime dimer mixtures derived from uracil aldehyde **1** and aryl aldehydes **13**−**17** is presented. No inhibition was observed for any oxime derived from **1** regardless of linker length (*n*). (B) Screen of oxime dimer mixtures derived from uracil aldehyde **3** and aryl aldehydes **13**−**17** is shown. The mixed oxime derived from **3** and **13** shows significant inhibition, and this derivative was further optimized. For **14**−**17**, the observed inhibition represents that from the **3**−**3** homodimers that are present in the mixtures.

none of the U∧U homodimers derived from **2** were found to be inhibitory, nor were any of the R∧R homodimers regardless of the linker length. (Inhibition by the homodimers is automatically assessed because these are present in multiple reaction mixtures.) In contrast, one oxime mixture derived from uracil aldehydes **2** and **3** and RCHO = 3,4-dihydroxybenzaldehyde (**13**) showed inhibitory activity in the range 15−100%, indicating that active heterodimers were present. The structures of the active heterodimers present in these two oxime mixtures are shown at the top of Table 1.

The two active mixtures were deconvoluted with respect to linker length by individually synthesizing each oxime dimer using a *single* diaminoalkanediol linker/reaction (Table 1). At this stage we did not separate the homodimers from the active heterodimers in the mixtures. For the oxime dimers derived from 5-formyluracil (**2**) and 3,4-dihydroxybenzaldehyde (**13**), a broad dependence on linker length was observed with length $n = 2$ being most favorable for inhibitory activity (i.e. mixed oxime **2**-(*2*)-**13**, Chart 1). In contrast, a very stringent linker length of $n = 3$ was required for maximal inhibitory activity with the oxime mixture derived from 6-formyluracil (**3**) and 3,4-dihydroxybenzaldehyde (**13**) to form mixed-oxime **3**-(*3*)-**13** (Chart 1). To confirm these results, **2**-(*2*)-**13** and **3**-(*3*)-**13** were separated from their respective homodimers using reversed phase HPLC (see Methods), and the concentration dependence of inhibition was determined. The measured IC_{50} values for **2**-(*2*)-**13** and **3**-(*3*)-**13** were 5.8 and 1.1 μM, respectively (Figure 5).

Structure−Activity Relationships. In an effort to find more potent inhibitors based on the **3**-(*3*)-**13** scaffold, 25 commercially

Table 1. Structures of Active Heterodimers and Dependence of Inhibition on Linker Length[a]

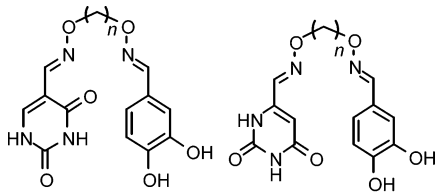

2-(*n*)-**13** **3**-(*n*)-**13**

mixture	linker length (*n*)	% inhibition
2-(*n*)-**13**	2	50
	3	40
	4	20
	5	20
	6	15
3-(*n*)-**13**	2	57
	3	100
	4	51
	5	48
	6	48

[a] Reactions were performed in the presence of 100 μM oxime mixture and 50 nM substrate concentration.

Chart 1. Heterodimer Oximes Identified from Deconvolution of an Active Mixture

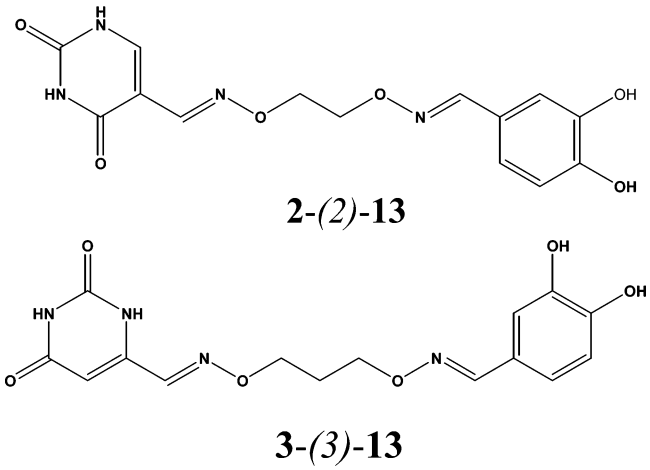

2-(*2*)-**13**

3-(*3*)-**13**

available benzaldehyde precursors were purchased (**18**−**42**; cf. Supporting Information Table S2). The HTP screen was then performed on this set of oxime mixtures (**3**-(*3*)-***R***) in an identical fashion as described above. This structure−activity study established that the 3- and 4-hydroxyl groups of **3**-(*3*)-**13** were essential for activity because alkylation or halogen substitution at these positions had a substantial deleterious effect on inhibitory activity (see Supporting Information Table S2). Thus,

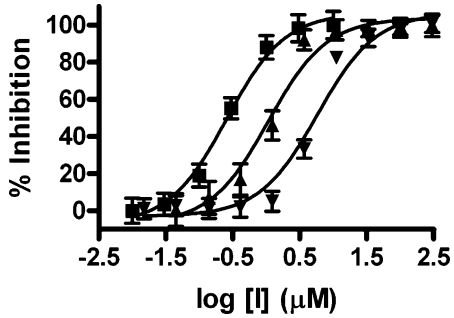

Figure 5. IC_{50} analysis for **2**-(*2*)-**13** (▼), **3**-(*3*)-**13** (▲), and **3**-(*3*)-**27** (■).

Table 2. Inhibitory Activity for Structural Variants of **3**-(*3*)-**27**[a]

3-*(3)*-***R***

RCHO =

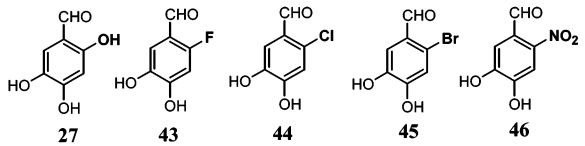

27 **43** **44** **45** **46**

variant	IC_{50} (μm)	2-R
3-(*3*)-**27**	0.26	OH
3-(*3*)-**43**	2.7	F
3-(*3*)-**44**	16	Cl
3-(*3*)-**45**	40	Br
3-(*3*)-**46**	40	NO_2

[a] The concentration dependence of inhibition was determined using 50 nM substrate.

hydrogen bond donating groups at the 3- and 4-positions of the benzyl ring appear to be essential.

One compound in this series with an additional hydroxyl group at the 2-position of the benzyl ring (**3**-(*3*)-**27**) showed a

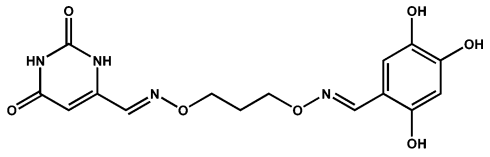

3-*(3)*-**27**

3-fold greater potency than **3**-(*3*)-**13** (Figure 5, ■) (IC_{50} = 0.3 μM). To further investigate SARs based around the **3**-(*3*)-**27** scaffold**,** we synthesized four more 3,4-dihydroxybenzaldehyde analogues (**43**−**46**, Table 2), where the substituent at the 2-position was varied (R = F, Cl, Br, or NO_2). Within this series there was a strong trend correlating with atomic size for the halogens, with the smaller fluorine substituent binding 16-fold more tightly than bromine. However, no substituent in this series was more effective than the 2-hydroxyl group. In conclusion, the binding pocket for the 2-substituent favors a hydrogen bond donating group with a van der Waals radius smaller than chlorine.

Inhibition Mechanisms of 3-(*3*)-27, 2-(*2*)-13, and Uracil. Although the uracil-directed ligand tethering strategy is expected to produce competitive inhibitors of UNG, we thoroughly investigated whether this assumption was true. The detailed mode of inhibition by **3**-(*3*)-**27** and **2**-(*2*)-**13** was evaluated by varying both substrate and inhibitor concentrations (Figure 6A,B). Standard double reciprocal plots of $1/k_{obsd}$ against 1/[DNA] at increasing concentrations of **3**-(*3*)-**27** showed no significant intercept effects establishing a competitive aspect to the inhibition (Figure 6A). However, a secondary plot of the Lineweaver−Burk slopes against [**3**-(*3*)-**27]** showed a *parabolic* response consistent with the presence of at least two inhibitor binding sites (Figure 6A, inset).[36] Global discrimination fitting of the inhibition data by computer simulation with the program Dynafit using competitive, noncompetitive, uncompetitive, mixed-type, two-site competitive−noncompetitive, and two-site competitive−uncompetitive inhibition mechanisms unambiguously confirmed the presence of two inhibitory binding sites for **3**-(*3*)-**27** (see Supporting Information).[37] Simulations clearly indictated that the first tight site is competitive with respect to substrate. Although the simulations indicated a slight statistical advantage for a partial mixed-type inhibition mode for the second weaker site, it was difficult to eliminate an uncompetitive mode for this site. Using the criterion of Occam's razor, the inhibition parameters for **3**-(*3*)-**27** are reported in Table 3 using the simulation results for the competitive−partial uncompetitive mechanism (Scheme 1).

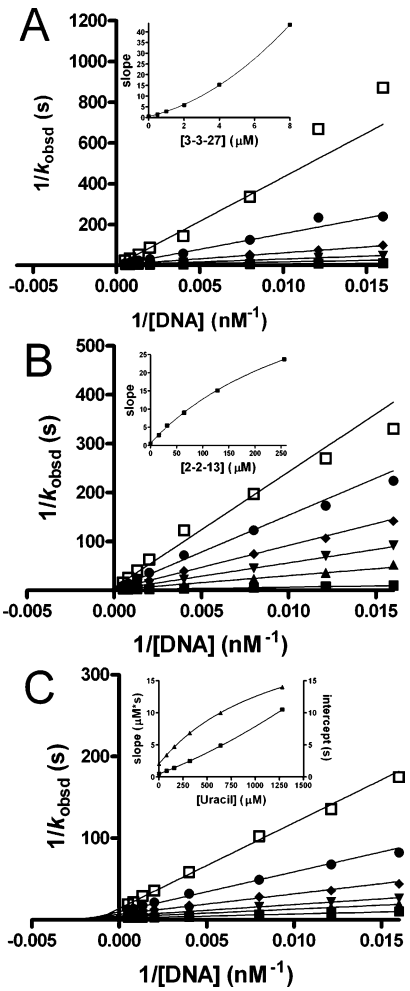

Figure 6. Mode of inhibition analysis, presenting double reciprocal plots and secondary slope and intercept replots for inhibition by increasing concentrations of (A) **3**-(*3*)-**27**, (B) **2**-(*2*)-**13**, and (C) uracil. Slope and intercept effects in the inset to (C) are shown as squares and triangles, respectively.

Like its 6-substituted analogue, initial inspection of the Lineweaver−Burk analysis of **2**-(*2*)-**13** indicates mixed-type inhibition with a strong preference for binding to the free enzyme (i.e. slope effects, Figure 6B). However, in contrast to **3**-(*3*)-**27**, the secondary plot of the Lineweaver−Burk slopes versus **2**-(*2*)-**13** concentration is *hyperbolic*, indicating that binding of **2**-(*2*)-**13** results in partial inhibition (Figure 6B, inset).[36] Because binding to the active site would result in complete inhibition, **2**-(*2*)-**13** most likely binds to the noncompetitive site observed for **3**-(*3*)-**27.** Global discrimination fitting of the inhibition data by computer simulation confirmed this inhibition mechanism (Scheme 1) and provided the inhibition

(36) Segel, I. H. *Enzyme Kinetics*; John Wiley & Sons: New York, 1993; Chapter 8, pp 465−504.

(37) Kuzmic, P. *Anal. Biochem.* **1996**, *237*, 260−273.

Table 3. Inhibition Constants for Uracil and Its Derivatives[a]

param	**3**-(*3*)-**27**	**2**-(*2*)-**13**	uracil	**51**
K_s (mM)	0.19 ± 0.02	0.23 ± 0.03	0.23 ± 0.02	0.16 ± 0.01
k_{cat} (s^{-1})	0.41 ± 0.01	0.50 ± 0.02	0.47 ± 0.01	0.33 ± 0.01
k_{cat} (s^{-1})	0.16 ± 0.04	0.012 ± 0.02	0.06 ± 0.01	
K_c (mM)	0.32 ± 0.02		80 ± 7	45 ± 2
K_n (mM)		2.8 ± 0.1		
K_n^c (mM)	1.2 ± 0.2		300 ± 55	
K_n^s (μM)	1 ± 0.3	125 ± 46	104 ± 7	
mode of inhibitn	two sites, competitive, partial uncompetitive	one site, partial mixed-type	two sites, competitive, partial uncompetitive	one site, competitive

[a] Parameters correspond to the mechanisms shown in Scheme 1. K_c and K_n represent dissociation constants for inhibitor binding sites that are competitive and noncompetitive with substrate, respectively. K_n^c and K_n^s represent the dissociation constants for inhibitor binding to the noncompetitive site when the active site is occupied by the competitively bound inhibitor or substrate, respectively. In these simulations the Michaelis−Menten parameters for the substrate were fixed using values from nonlinear regression fits (Figure 6). Other parameters were obtained from simulations to the data using the program Dynafit (cf. Supporting Information).

Scheme 1. Inhibition Mechanisms for **3**-(*3*)-**27** and **2**-(*2*)-**13** and Uracil[a]

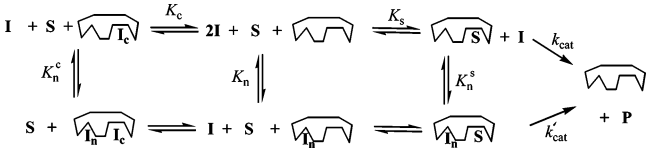

[a] Only **3**-(*3*)-**27**, **2**-(*2*)-**13**, and uracil have mechanisms that include the k_{cat}' step. The mechanisms for **3**-(*3*)-**27** and uracil do not include the equilibrium constant K_n, and the mechanism for **2**-(*2*)-**13** does not include the equilibria K_c or K_n^c.

constants reported in Table 3. These observations strongly indicate that **2**-(*2*)-**13** binds to a site distinct from the active site, although DNA binding is strongly antagonistic to inhibitor binding (Table 3). In summary, the inhibition mechanisms of **3**-(*3*)-**27** and **2**-(*2*)-**13** indicate that two inhibition modes exist for these uracil derivatives: one mode competitively targets the active site, and the second weaker mode is noncompetitive or uncompetitive with respect to substrate binding. These data, quite surprisingly, suggested the presence of two uracil binding sites on human UNG.

To further investigate the interesting possibility of two uracil binding sites on UNG, we performed a mode of inhibition analysis for uracil itself (Figure 6C). In confirmation of this initial expectation, inhibition by uracil involves two sites. The first site is competitive, and the second is partially uncompetitive. Accordingly, the Lineweaver−Burk slope replot was slightly parabolic indicating that inhibition involved binding of more than one molecule of uracil, and the intercept replot was hyperbolic indicating a partial uncompetitive mode. These characteristics of the inhibition by uracil combine the features observed for **3**-(*3*)-**27** and **2**-(*2*)-**13** and establish that the two site binding of **3**-(*3*)-**27** is not attributable to the trihydroxybenzaldoxime moiety but, instead, arises from the uracil functionality itself.

Implications for Two Uracil Binding Sites. Why would UNG have a second uracil binding site? Although the answer to this question cannot be firmly established by inhibition data alone, an intriguing role for this site during the mechanism of uracil base flipping is supported by several different experimental findings. First, kinetic experiments following the pathway of uracil flipping from duplex DNA have detected a weakly bound intermediate state of uracil that precedes its attainment of the final extrahelical state seen in the crystal structure (Figure 1A).[15,38−40] Solution- and solid-state NMR studies of uracil flipping support the existence of a weak uracil binding site because UNG is found to transiently stabilize thymine and other uracil congeners in an extrahelical conformation, without these bases gaining full access to the uracil active site pocket.[41,42] Relevant to these observations, the crystal structure of herpesvirus UDG bound to pTTTp shows that the 5′ T is bound in the mouth of the active site pocket in a manner that is consistent with a transient state on the pathway for base flipping of uracil.[43] Finally, the crystal structure of another base-flipping DNA repair enzyme, human 8-oxoguanine DNA glycosylase, suggests that this related enzyme can flip the normal base guanine into a discrimination pocket that was distinct from the active site pocket that only accommodates 8-oxoguanine.[44] These combined data provide a compelling case for a generalized pathway for base flipping involving transient enzyme stabilization of at least one extrahelical intermediate state before the base is docked into the active site. On the basis of the observation that **2**-(*2*)-**13** is excluded from the active site but that **3**-(*3*)-**27** and uracil can occupy both sites**,** we surmise that the relative binding affinities for each site might depend on the bulkiness of the substituent at the 5-position of uracil. In other words, uracil congeners with small substituents at the five position (such as hydrogen in the case of **3**-(*3*)-**27**) would favor binding to the active site and uracil derivatives with bulkier substituents (such as the dihydroxybenzaldoxime of **2**-(*2*)-**13**) would be sterically excluded from the active site but could gain access to the weaker less selective site. Indeed, it is well-known that the active site of UNG uses the bulky side chain of a tyrosine to exclude thymidine (5-methyluracil),[14,45−47] yet 6-substituted uracil derivatives such as **3**-(*3*)-**27** have been generally observed to bind to the active site.[14] Thus, the uracil-based inhibitors found here have revealed a possible pyrimidine discrimination site that may be employed during the multistep extrahelical uracil recognition mechanism. It should be noted that the noncompetitive inhibition

(38) Jiang, Y. L.; Kwon, K.; Stivers, J. T. *J. Biol. Chem.* **2001**, *276*, 42347−42354.
(39) Jiang, Y. L.; Song, F.; Stivers, J. T. *Biochemistry* **2002**, *41*, 11248−11254.
(40) Jiang, Y. L.; Stivers, J. T. *Biochemistry* **2002**, *41*, 11236−11247.
(41) Cao, C.; Jiang, Y. L.; Stivers, J. T.; Song, F. *Nat. Struct. Mol. Biol.* **2004**, *11*, 1230−1236.
(42) Jiang, Y. L.; McDowell, L.; Poliks, B.; Studelska, D.; Cao, C.; Potter, G. S.; Schaefer, J.; Song, F.; Stivers, J. T. *Biochemistry* **2004**, *43*, 15429−15438.
(43) Savva, R.; McAuley-Hecht, K.; Brown, T.; Pearl, L. *Nature* **1995**, *373*, 487−493.
(44) Banerjee, A.; Yang, W.; Karplus, M.; Verdine, G. L. *Nature* **2005**, *434*, 612−618.
(45) Kavli, B.; Slupphaug, G.; Mol, C. D.; Arvai, A. S.; Peterson, S. B.; Tainer, J. A.; Krokan, H. E. *EMBO J.* **1996**, *15*, 3442−3447.
(46) Mol, C. D.; Arvai, A. S.; Slupphaug, G.; Kavli, B.; Alseth, I.; Krokan, H. E.; Tainer, J. A. *Cell* **1995**, *80*, 869−878.
(47) Kwon, K.; Jiang, Y.; Stivers, J. *Chem. Biol.* **2003**, *10*, 1−20.

Chart 2. *O*-Methyl Oxime Derivatives of the Aldehyde Binding Elements of **2**-(*2*)-**13** and **3**-(*3*)-**27**

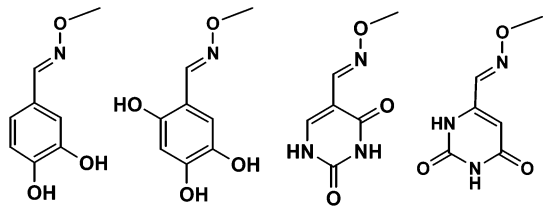

47 **48** **50** **51**

mode for **2**-(*2*)-**13** requires that the final extrahelical state can be attained, albeit inefficiently, even when the transient uracil binding site is occupied by the inhibitor. In contrast, the partial uncompetitive mechanism for binding of **3**-(*3*)-**27** to its second site does not present the same apparent discrepancy, because, for uncompetitive inhibition, the compound binds after the substrate is fully inside the active site pocket (see above).

Inhibition by the Untethered Parts. It is of interest to ask how well uracil-directed ligand tethering has performed. To dissect the energetic contributions of the formyluracil and hydroxybenzaldoxime binding elements of **3**-(*3*)-**27** and **2**-(*2*)-**13,** we synthesized the methyl oxime derivatives of aldehydes **2**, **3**, **27**, and **13** as shown in Chart 2. These methyl oxime derivatives are reasonable mimics of the two individual binding elements and in principle could provide an energetic analysis of the binding affinities of the two separate elements. If the sum of the binding energies of each element equals the entire binding free energy of the whole tethered molecule, then it may be concluded that (i) the tether is energetically inert with respect to binding and (ii) the binding of one element does not affect the other by induced strain or forcing a tighter fit. If the whole tethered molecule binds much more weakly or tightly than expected from the summation of the binding free energies of the two individual binding elements, then nonadditive energetic effects are present. Such effects would indicate either an energetic penalty for tethering (antagonistic binding of the parts) or, alternatively, a nonadditive energetic benefit (synergistic binding of the parts).[48,49]

Comparison of the binding affinity of **3**-(*3*)-**27** to its competitive site ($K_c^{\mathbf{3}-(3)-\mathbf{27}} = 0.32\ \mu$M) with that of the 6-formyluracil *O*-methyl oxime binding element alone (**51)** allows estimation of the free energy benefit of tethering the trihydroxybenzaldoxime binding element to the 6-formyluracil oxime part. Conversely, comparison of the binding affinity of **3**-(*3*)-**27** with that of the trihydroxybenzaldoxime *O*-methyl ether (**48)** allows estimation of the free energy benefit of tethering the 6-formyluracil oxime binding element to the trihydroxybenzaldoxime part. The 6-formyluracil *O*-methyl oxime **51** shows a cleanly competitive mode of inhibition with $K_c^{\mathbf{51}} = 45 \pm 2\ \mu$M (Table 4, data not shown). Thus, the enhancement in the free energy of binding upon addition of the trihydroxybenzaldoxime (THB) part to the 6-formyluracil oxime element is $\Delta\Delta G^{\mathrm{THB}} = -RT \ln(K_i^{\mathbf{3}-(3)-\mathbf{27}}/K_i^{51}) = -3$ kcal/mol. We were unable to perform a similar energetic analysis with the trihydroxybenzaldoxime *O*-methyl ether (**48**) due to its extremely weak binding (9% inhibition at 1 mM concentration, data not shown). Similarly, an energetic analysis of the binding elements comprising **2**-(*2*)-**13** was not possible because of the extremely weak inhibition by the 5-formyluracil *O*-methyl oxime (**50**) and the dihydroxybenzaldoxime *O*-methyl ether (**47**). Nevertheless, the 140-fold greater binding affinity of **3**-(*3*)-**27** as compared to the 6-formyluracil *O*-methyl oxime binding element (**51**) alone indicates that a large benefit can be derived from tethering.[50]

Experimental Section

Reagents and General Methods. All chemicals were purchased from commercial sources without further purification unless otherwise stated. The ^{1}H, ^{13}C, and ^{19}F NMR spectra were recorded on a 400 MHz Varian Innova instrument. The spectra were recorded in deuteriochloroform ($CDCl_3$) or in hexadeuteriodimethyl sulfoxide (DMSO-d_6). The chemical shifts of protons are given in ppm with TMS as internal standard. The chemical shifts of carbons are obtained in ppm with solvents as internal standards. That of fluorine is given in ppm with 1% trifluoroacetic acid in DMSO-d_6 as an external standard. Most of oximes were purified by HPLC using aqueous triethylammonium acetate (TEAA) as a running buffer. Therefore, TEAA was not completely removed and it appeared in the NMR spectra. Accordingly, proton and carbon chemical shifts of TEAA were not listed during the characterizations of the oximes. During the purification of the oxime **3**-(*3*)-**27**, 2-mercaptoethanol was used as an antioxidant. Therefore, small amounts of this compound and its oxidation product are also present in the oxime **3**-(*3*)-**27**. Flash chromatographies were performed with silica (70−230 mesh from Sorbent Technologies) and monitored by thin-layer chromatography (TLC) with silica plates (Merck, Kieselgel 60 F254).

Synthesis of Alkyl Hydroxyamines. *O*,*O*′-Diaminoalkanediol linkers of variable length (ethyl, propyl, butyl, pentyl, hexyl) were prepared from the corresponding dibromoalkanes in two steps according to literature procedures (Figure 2A).[33,51,52]

General Synthesis of Tethered Oxime Dimers. A set of 14 aryl aldehydes (**4**−**17**; cf. Supporting Information Table S1) was selected for library synthesis for coupling to the three uracil containing aldehydes (**1**−**3**, Figure 2) using the *O*,*O*′-diaminoalkanediol linkers as follows. To each 0.5-mL well of a Matrix microtiter plate was added a DMSO stock solution of AcOH (20 μL, 150 mM, 3 μmol), uracil aldehyde **1**−**3** (20 μL, 150 mM, 3 μmol), and a single aryl aldehyde (20 μL, 150 mM, 3 μmol). The plate was carefully agitated to make the solutions homogeneous. To each of the uracil−aryl aldehyde mixture was added a DMSO solution of the *O*,*O*′-diaminoalkanediol linkers containing each of the five linker lengths in equal proportion (22 μL, 150 mM, 3.3 μmol total amine equivalents). The plate was sealed, further agitated, and incubated in an oven for 12 h at 37 °C.

The most potent inhibitors from this first screen **2**-(*2*)-**13** and **3**-(*3*)-**13**) were synthesized in larger scale and thoroughly characterized after HPLC purification of the heterodimers as follows.

2-(*2*)-13: ^{1}H NMR (400 MHz, DMSO-d_6) δ 8.05 (s, 1 H), 7.91 (s, 1 H), 7.78 (s, 1 H), 7.04 (s, J = 2.4 Hz, 1 H), 6.86 (m, 1 H), 6.74 (d, J = 8.0 Hz, 1 H), 4.26 (s, 1 H); ^{13}C NMR (100 MHz, DMSO-d_6) δ 162.40, 151.04, 149.25, 147.92, 145.75, 142.74, 140.66, 123.05, 119.88, 115.74, 113.10, 104.31, 71.82, 71.54; UV/vis λ_{max} 275 nm; HRMS (*m*/*z*) [M + Na]$^+$ calcd for $C_{14}H_{14}N_4O_6Na$ 357.08, found 357.08.

3-(*3*)-13: ^{1}H NMR (400 MHz, DMSO-d_6) δ 9.10 (bs, H), 8.01 (s, 1 H), 7.94 (s, 1 H), 7.04 (d, J = 1.6 Hz, 1 H), 6.82 (d, J = 7.6 Hz, 1 H), 6.74 (d, J = 7.6 Hz, 1 H), 5.78 (s, 1 H), 4.26 (t, J = 6.8 Hz, 2 H), 4.12 (t, J = 6.0 Hz, 2 H), 2.06 (t, J = 6.8 Hz, 2 H); ^{13}C NMR (125 MHz,

(48) Page, M. I.; Jencks, W. P. *Proc. Natl. Acad. Sci. U.S.A.* **1971**, *68*, 1678−1683.
(49) Jencks, W. P. Binding Energy, Specificity, and Enzymic Catalysis: The Circe Effect. In *Catalysis in Chemistry and Enzmology*; Dover Publications: New York, 1987; pp 615−807.
(50) The uracil N1-acetaldehyde *O*-methyl oxime (**49**) showed undetectable inhibition (K_c > 10 mM).
(51) Kung, P. P.; Bharadwaj, R.; Fraser, A. S.; Cook, D. R.; Kawasaki, A. M.; Cook, P. D. *J. Org. Chem.* **1998**, *63*, 1846−1852.
(52) Weiss, R. H.; Furfine, E.; Hausleden, E.; Dixon, D. W. *J. Org. Chem.* **1984**, *49*, 4969−4972.

DMSO-d_6) δ 163.95, 151.15, 148.96, 148.04, 145.89, 144.73, 142.23, 123.12, 119.83, 115.81, 113.15, 101.60, 71.94, 69.76, 28.46; UV/vis λ_{max} 273 nm; HRMS (*m*/*z*) $[M + H]^+$ calcd for $C_{15}H_{17}N_4O_6$ 349.11, found 349.11.

The second set of oxime dimers based on the **3**-(*3*)-**13** hit discovered in the first screening round were synthesized in an identical fashion as described above using uracil aldehyde **3** and hydroxybenzaldehydes **18**−**42** and the *O*,*O*′-diaminopropanediol linker (cf. Supporting Information Table S2). The most potent inhibitor identified from this second round of screening (**3**-(*3*)-**27**) was synthesized in larger scale and thoroughly characterized. **3**-(*3*)-**27**: ^{1}H NMR (400 MHz, DMSO-d_6) δ 9.10 (bs, H), 8.21 (s, 1 H), 7.94 (s, 1 H), 6.88 (s, 1 H), 6.31 (s, 1 H), 5.78 (s, 1 H), 4.28 (t, J = 6.0 Hz, 2 H), 4.10 (t, J = 6.0 Hz, 2 H), 2.06 (m, 2 H); ^{13}C NMR (125 MHz, DMSO-d_6) δ 163.91, 151.04, 150.25, 149.17, 146.90, 144.63, 142.20, 138.73, 112.76, 107.78, 103.56, 101.69, 71.90, 69.77, 28.38; UV/vis λ_{max} 286 nm; ESI (*m*/*z*) for $[M + H]^+$ calcd for $C_{15}H_{18}N_4O_7$ 366, found 366; ESI (*m*/*z*) for $[M + Na]^+$ calcd for $C_{15}H_{17}N_4O_7Na$ 388, found 388; ESI (*m*/*z*) for $[M - H]^-$ calcd for $C_{15}H_{16}N_4O_7$ 364, found 364.

Isolation and Purification of Oxime Dimers using HPLC. All of the most active oxime heterodimers were purified by HPLC using a Phenomenex Aqua reversed phase C-18 HPLC column (250 mm, 10 mm, 5 μm). Most of the oximes were purified using gradient elution from 0 to 30% CH_3CN in 0.1 M aqueous TEAA over the course of 2 h using UV detection at 254 nm. An exception was oxime **3**-(*3*)-**27**, which is prone to air oxidation. In this case, 25 mM 2-mercaptoethanol was added to both of the running buffers. The oximes all eluted with baseline resolution in the order U−U homodimer, U−R heterodimer, followed by the R−R homodimer. This HPLC method was also used to confirm the expected 1:2:1 stoichiometries of homodimer and heterodimer oxime formation, using 10 representative uracil and aryl aldehydes from the library (see Supporting Information Figure S1). Additional NMR evidence supporting the expected stoichiometries is detailed in the Supporting Information Figures S2 and S3.

Synthesis of 2-R-Substituted 3,4-Dihydroxybenzaldehydes and the Corresponding Mixed Oximes with 3. Aldehyde **43** was synthesized by removing the methyl groups of the commercially available 3,4-dimethoxy-6-fluorobenzaldehyde using BBr_3 in CH_2Cl_2.[53] The aldehydes **44** and **45** were synthesized by removing the methylene group of the corresponding 2-halogenated piperonal using $AlCl_3$ and 6N HCl.[54] Aldehyde **46** was commercially available. These four aldehydes (**43**−**46**) were reacted with 6-formyluracil **3** and the *O*,*O*′-diaminopropanediol linker using the procedure described above, and the mixed oxime dimer was obtained after HPLC purification.

3-(*3*)-**43:** ^{1}H NMR (400 MHz, DMSO-d_6) δ 8.11 (s, 1 H), 7.94 (s, 1 H), 7.05 (d, J = 7.2 Hz, 1 H), 6.58 (d, J = 6.8 Hz, 1 H), 5.77 (s, 1 H), 5.10 (bs, H), 4.28 (t, J = 6.8 Hz, 2 H), 4.16 (t, J = 6.0 Hz, 2 H), 2.07 (m, 2 H); ^{13}C NMR (125 MHz, DMSO-d_6) δ 163.91, 155.50, 153.09, 151.08, 149.87, 149.76, 144.65, 142.72, 142.30, 142.21, 110.91, 110.87, 108.62, 108.49, 103.21, 102.96, 101.67, 71.85, 70.06, 28.38; ^{19}F NMR (DMSO-d_6) δ −54.33, −54.35, −54.36, −54.38; UV/vis λ_{max} 268 nm; HRMS (*m*/*z*) $[M + Na]^+$ calcd for $C_{15}H_{15}FN_4O_6Na$ 389.09, found 389.09.

3-(*3*)-**44:** ^{1}H NMR (400 MHz, DMSO-d_6) δ 8.23 (s, 1 H), 7.94 (s, 1 H), 7.18 (s, 1 H), 6.77 (s, 1 H), 5.78 (s, 1 H), 4.27 (t, J = 5.6 Hz, 2 H), 4.16 (t, J = 6.0 Hz, 2 H), 2.08 (m, 2 H); ^{13}C NMR (125 MHz, DMSO-d_6) δ 163.90, 151.08, 149.71, 145.48, 145.16, 144.64, 142.21, 123.00, 119.09, 116.08, 112.33, 101.67, 71.85, 70.22, 28.37; UV/vis λ_{max} 275 nm; HRMS (*m*/*z*) $[M + Na]^+$ calcd for $C_{15}H_{15}ClN_4O_6Na$ 405.06, found 405.06.

3-(*3*)-**45:** ^{1}H NMR (400 MHz, DMSO-d_6) δ 8.18 (s, 1 H), 7.94 (s, 1 H), 7.19 (s, 1 H), 6.93 (s, 1 H), 5.78 (s, 1 H), 4.27 (t, J = 6.4 Hz, 2 H), 4.16 (t, J = 6.4 Hz, 2 H), 2.08 (m, 2 H); ^{13}C NMR (125 MHz, DMSO-d_6) δ 163.91, 151.10, 150.07, 147.41, 146.02, 144.66, 142.22, 120.58, 119.15, 112.89, 112.29, 101.69, 71.86, 70.24, 28.38; UV/vis λ_{max} 278 nm; HRMS (*m*/*z*) $[M + Na]^+$ calcd for $C_{15}H_{15}BrN_4O_6Na$ 449.01, found 449.01.

3-(*3*)-**46:** ^{1}H NMR (400 MHz, DMSO-d_6) δ 8.56 (d, J = 1.2 Hz, 1 H), 7.95 (s, 1 H), 7.37 (s, 1 H), 6.74 (s, 1 H), 6.26 (bs, H), 5.78 (d, J = 1.2 Hz, 1 H), 4.28 (t, J = 6.0 Hz, 2 H), 4.16 (t, J = 6.0 Hz, 2 H), 2.09 (m, 2 H); ^{13}C NMR (125 MHz, DMSO-d_6) δ 163.88, 160.27, 151.05, 148.62, 148.00, 144.62, 142.22, 133.36, 122.38, 113.80, 109.23, 101.73, 71.85, 70.07, 28.39; UV/vis λ_{max} 269 nm; HRMS (*m*/*z*) $[M + H]^+$ calcd for $C_{15}H_{16}N_5O_8$ 394.10, found 394.10.

Synthesis of Methyl Oxime Derivatives of 1−3, 13, and 27. The *O*-methyl oxime of 3,4-dihydroxybenzaldehyde (**47**) is known and was synthesized using **13** and *O*-methylhydroxylamine hydrochloride.[55] *O*-Methyloximes **48**−**51** were made using a similar method.

48: To a solution of **27** (308 mg, 2.0 mmol) in 4.0 mL of EtOH−H_2O−THF (0.45/0.3/0.25) were added sodium acetate (264 mg) and *O*-methylhydroxylamine hydrochloride (183 mg), and the solution was stirred at room temperature for overnight. The solvents were removed in vacuo, and the residue was extracted with chloroform three times. The combined organic layers were dried over anhydrous $MgSO_4$ and concentrated in vacuo. The residue was purified by silica gel column chromatography (EtOAc/hexanes) to give a product amount of 347 mg in 95% yield: ^{1}H NMR (400 MHz, DMSO-d_6) δ 9.38 (s, 1 H), 9.21 (s, 1 H), 8.52 (s, 1 H), 8.18 (s, 1 H), 6.88 (s, 1 H), 6.30 (s, 1 H), 3.80 (s, 3 H); ^{13}C NMR (125 MHz, DMSO-d_6) δ 150.17, 148.88, 146.52, 138.61, 112.51, 107.77, 103.46, 61.28; UV/vis λ_{max} 239, 274 nm; HRMS (*m*/*z*) $[M + H]^+$ calcd for $C_8H_{10}NO_4$ 184.06, found 184.06.

49: To a solution of **1** (10.8 mg, 0.063 mmol) in hot DMF (0.5 mL) were added sodium acetate (5.2 mg, 0.063 mmol) solution in water (0.1 mL) and *O*-methylhydroxylamine hydrochloride (5.3 mg, 0.063 mmol), and the solution was stirred at room temperature for overnight. The solvents were removed in vacuo, and the residue was purified by column chromatography using 10−15% (v/v) methanol in CH_2Cl_2, resulting in 90% yield (10.3 mg 50/50 mixture of trans and cis geometric isomers): ^{1}H NMR (400 MHz, chloroform-*d*) δ 9.56 (s, 1 H), 7.43 (t, J = 5.2 Hz,0.5 H), 7.20 (m, 1 H), 6.80 (t, J = 4.4 Hz,0.5 H), 5.78 (m, 1 H), 4.55 (d, J = 4.4 Hz,1 H), 4.48 (d, J = 5.6 Hz,1 H), 3.94 (s, 1.5 H), 3.87 (s, 1.5 H); ^{13}C NMR (100 MHz, DMSO-d_6) δ 163.92, 163.87, 151.06, 150.99, 144.72, 144.54, 143.93, 143.53, 103.14, 102.97, 62.68, 62.37, 46.52, 43.76; UV/vis λ_{max} 263 nm; HRMS (*m*/*z*) $[M + H]^+$ calcd for $C_7H_{10}N_3O_3$ 184.07, found 184.07.

50: To a solution of **2** (70 mg, 0.5 mmol) in hot DMF (1 mL) were added sodium acetate (41 mg, 0.5 mmol) solution in water (0.5 mL) and *O*-methylhydroxylamine hydrochloride (42 mg, 0.5 mmol), and the solution was stirred at room temperature for 4 h. The solvents were removed in vacuo, and the residue was collected by filtration and washed with cold water 2 × 1 mL, resulting in 76% yield (70 mg 87/13 mixture of trans and cis geometric isomers): ^{1}H NMR (400 MHz, DMSO-d_6) δ 11.40 (bs, 2 H), 8.52 (s, 0.13 H), 7.87 (s, 0.87 H), 7.74 (s, 0.87 H), 7.29 (s, 0.13 H), 3.89 (s, 0.39 H), 3.80 (s, 2.61 H); ^{13}C NMR (100 MHz, DMSO-d_6) δ 162.98, 162.36, 150.80, 150.27, 146.08, 142.26, 140.09, 137.31, 104.41, 103.43, 62.32, 61.44; UV/vis λ_{max} 288 nm; HRMS (*m*/*z*) $[M + H]^+$ calcd for $C_6H_8N_3O_3$ 170.06, found 170.06.

51: To a solution of **3** (79 mg, 0.5 mmol) in hot DMF (2.0 mL) were added sodium acetate (46 mg, 0.5 mmol) solution in water (0.5 mL) and *O*-methylhydroxylamine hydrochloride (46 mg, 0.5 mmol), and the solution was stirred at 50 °C for 4 h. The solvents were removed in vacuo, and the residue was washed by cold water. After the filtration, product was obtained in 62% yield (53 mg): ^{1}H NMR (400 MHz, DMSO-d_6) δ 11.18 (s, 1 H), 10.77 (s, 1 H), 7.91 (s, 1 H), 5.77 (s, 1 H), 3.96 (s, 3 H); ^{13}C NMR (125 MHz, DMSO-d_6) δ 163.87, 151.02,

(53) Kirk, K. L.; Cantacuzene, D.; Nimitkitpaisan, Y.; Mcculloh, D.; Padgett, W. L.; Daly, J. W.; Creveling, C. R. *J. Med. Chem.* **1979**, *22*, 1493−1497.
(54) Reitz, A.; Avery, M. A.; Verlander, M. S.; Goodman, M. *J. Org. Chem.* **1981**, *46*, 4859−4863.
(55) Watanabe, T.; Suzuki, T.; Umezawa, Y.; Takeuchi, T.; Otsuka, M.; Umezawa, K. *Tetrahedron* **2000**, *56*, 741−752.

144.51, 142.17, 101.41, 62.84; UV/vis λ_{max} 292 nm; HRMS (*m*/*z*) [M + Na]$^+$ calcd for $C_6H_7N_3O_3Na$ 192.04, found 192.04.

High-Throughput Inhibitor Screening. The substrate in this HTS assay was synthesized using standard phosphoramidite DNA solid-phase chemistry using reagents purchased from Glen Research. The DNA was purified using anion exchange chromatography followed by desalting using reversed phase methods. The sequence and size was confirmed using analytical denaturing polyacrylamide gel electrophoresis and MALDI-MS. The substrate is a double-stranded 14-mer DNA containing nine U·A base pairs (5′-FAM-GCA CUU AAG AAU UG: 3′-DABSYL-CA AUU CUU AAG UGC). The UNG HTS assay is performed as follows. To a 96-well microtiter plate was added 5 μL (2 mM total) of compound in DMSO, followed by 75 μL (33.3 pM) of human UNG in reaction buffer (10 mM Tris·HCl, pH 8.0, 20 mM NaCl, 7.5 mM $MgCl_2$, 0.002% brij-35). The reactions were initiated by the addition of 20 μL (250 nM) of molecular beacon substrate in reaction buffer. The plates are incubated at ambient temperature in a fluorescence plate reader for 30 min, and the progress of the reaction was monitored every 5 min (ex 485 nm/em 520 nm). The final concentrations of the reagents in the assay are 10 mM Tris·HCl, pH 8.0, 20 mM NaCl, 7.5 mM $MgCl_2$, 0.002% Brij-35, 25 pM human UNG, 50 nM molecular beacon substrate, 100 μM total compound, and 5% DMSO. The $MgCl_2$ is essential to increase the stability of the double-stranded DNA substrate and, thus, decrease the initial fluorescence of the molecular beacon and increase the maximum signal of the assay. Addition of Brij-35, a nonionic detergent, is essential to stabilize human UNG at the low concentration used in this assay. A similar assay has been described by Maksimenko et al. that utilizes a 39-mer hairpin DNA.[56] However, the synthesis and purification of this more complex substrate proceeds with low efficiency and requires higher temperature to induce strand separation (Krosky and Stivers, unpublished data). In contrast, the 14-mer double-stranded molecular beacon is routine and allows screening to be performed conveniently at room temperature.

Mechanism of Inhibition. The substrate used in mechanism of inhibition studies was a modified DNA hairpin where the two strands described above are connected by a hexakis[poly(ethylene glycol)} linker (PEG-U9). This substrate was easier to synthesize and purify than an all-DNA hairpin and, unlike the double stranded DNA substrate, does not require $MgCl_2$ to achieve minimum fluorescence. To a 96-well plate was added 5 μL of compound in DMSO, followed by 75 μL of PEG-U9 hairpin in reaction buffer (20 mM Tris·HCl, pH 8.0, 50 mM KCl, 0.2 mM $MgCl_2$, 0.002% Brij-35, 1 mM DTT). Eight different DNA concentrations were used in the range 62.5−2000 nM. Reactions were initiated by the addition of 20 μL of 0.5 nM human UNG in reaction buffer. The final concentrations of reagents in the assay are 20 mM Tris·HCl, pH 8.0, 50 mM KCl, 0.2 mM $MgCl_2$, 0.002% Brij-35, 1 mM DTT, 5% DMSO, 0.1 nM human UNG, 62.5−2000 nM PEG-U9 hairpin DNA, and variable amounts of inhibitor. The plates were incubated at ambient temperature in a fluorescence plate reader for 60 min, and the progress of each reaction was monitored every 5 min (ex 485 nm/em 520 nm). Afterward, *Escherichia coli* UNG was added to each well to drive the reactions to completion, and the overall change in fluorescence values were measured. These values were used to convert initial velocities from units of fluorescence units/s to [product]/s. Mechanisms of inhibition and their corresponding inhibitor dissociation constants were determined by Lineweaver−Burk slope and intercept replot analysis and by computational simulations of the initial velocity against inhibitor concentration data using Dynafit v.3.28 (see Supporting Information)

Conclusions

We have developed an efficient strategy to develop small-molecule inhibitors of UNG that have the potential for activity in cell culture or in vivo. The method is quite general and could be adapted to target other enzymes that bind extrahelical bases or free nucleosides. Two future targets of the current uracil mixed oxime library would be the essential bacterial enzyme deoxyuridine nucleotidylhydrolase, which converts dUTP to dUMP,[23,57−60] and human thymidine phosphorylase, an enzyme implicated in vascularization of tumors.[61] Such inhibitors could serve as useful tools to study the life cycle of pathogenic human viruses, the biology of uracil base excision repair in normal cell lines and tissues, and mechanisms of tumor vascularization.

Acknowledgment. This work was supported by NIH Grant GM56834-10 to J.T.S. D.J.K was supported by the DOD Breast Cancer Research Program (Grant DAMD17-03-1-1251).

Supporting Information Available: Tables of aryl aldehydes and hydroxybenzaldehydes used to construct oxime libraries, HPLC traces and NMR spectra to ascertain stoichiometries of oxime mixtures, ^{1}H and ^{13}C NMR spectra of **3**-(*3*)-**13** and **3**-(*3*)-**27**, computer simulations of inhibition data, and analytical equations for each inhibition mechanism. This material is available free of charge via the Internet at http://pubs.acs.org.

JA055846N

(56) Maksimenko, A.; Ishchenko, A. A.; Sanz, G.; Laval, J.; Elder, R. H.; Saparbaev, M. K., *Biochem. Biophys. Res. Commun.* **2004**, *319*, 240−246.
(57) Grasser, F. A.; Romeike, B. F.; Niedobitek, G.; Nicholls, J.; Kremmer, E. *Curr. Protein Pept. Sci.* **2001**, *2*, 349−360.
(58) Hidalgo-Zarco, F.; Gonzalez-Pazanowska, D. *Curr. Protein Pept. Sci.* **2001**, *2*, 389−397.
(59) Studebaker, A. W.; Balendiran, G. K.; Williams, M. V. *Curr. Protein Pept. Sci.* **2001**, *2*, 371−379.
(60) Williams, M. V. *Virology* **1988**, *166*, 262−264.
(61) Toi, M.; Atiqur Rahman, M.; Bando, H.; Chow, L. W. *Lancet Oncol.* **2005**, *6*, 158−166.